Excited-State Potential Surface Crossings in Acrolein: A Model for Understanding the Photochemistry and Photophysics of α,β-Enones

Mar Reguero,† Massimo Olivucci,*,‡ Fernando Bernardi, and Michael A. Robb*,†

Contribution from the Dipartimento di Chimica "G. Ciamician" dell'Universita di Bologna, Via Selmi 2, 40126 Bologna, Italy, and Department of Chemistry, King's College, London, Strand, London WC2R 2LS, U.K

Received July 19, 1993. Revised Manuscript Received November 29, 1993•

Abstract: The interplay between the ground- and the three low-lying singlet/triplet excited-state surfaces (S_1, T_2, and T_1) in *s-trans*- and *s-cis*-acrolein has been studied using CASSCF computations at the 6-31G* level. The objective is to provide a model for understanding α,β-enone photochemistry and photophysics. Two different photochemically active relaxation paths starting from a planar S_1 $^1(n-\pi^*)$ excited state minimum have been documented. The first of these pathways involves a radiationless decay via intersystem crossing to the triplet manifold, leading to production of a short-lived T_1 $^3(\pi-\pi^*)$ twisted intermediate. This intermediate then decays, via a second intersystem crossing, to the ground state, leading to isomerization of the acrolein double-bond. The second relaxation path involves the singlet manifold only. In this case relaxation to S_0 occurs via a single decay channel which corresponds to a S_1/S_0 conical intersection. This conical intersection lies 15 and 10 kcal mol^{-1} above the $^1(n-\pi^*)$ *s-trans*- and $^1(n-\pi^*)$ *s-cis*-acrolein, respectively. Production of oxetene is found to occur via the singlet path starting exclusively from the S_1 $^1(n-\pi^*)$ *s-cis*-acrolein. The computational results agree well with the available experimental data. The existence of a T_1 $^3(\pi-\pi^*)$ intermediate is supported by the observation of a 280–310-nm transient absorption in both acyclic and cyclic α,β-enones. Further, the existence of a barrier to production of oxetene is in agreement with the fact that this product accumulates when acyclic α,β-enones are irradiated with light near 250 nm, but it is not detected when α,β-enones are irradiated near 300 nm.

Introduction

Many photochemical reactions are nonadiabatic. The reaction starts on an excited-state potential surface and proceeds ultimately to a bonding ground-state configuration via a surface crossing (where intersystem crossing or fast internal conversion takes place). Thus, the characterization of a mechanism of photochemical reaction involves, in addition to the study of ground- and excited-state reaction paths, a characterization of the region where the surface crossing occurs and the system decays nonradiatively to the ground state. For most photoreactions, it is still largely unknown at what point along the reaction coordinate the photoexcited reactant decays. However, this information is of central importance for understanding the nature and the yield of photoproducts which originate from a specific decay channel. The molecular structure of the system at the decay point determines, to a large extent, the possible final ground-state photoproducts associated with the corresponding decay channel. Thus, in photochemistry, a decay point plays a role similar to the transition state in thermal chemistry in the sense that the reacting system must pass through such points to reach the product. Recently, we have implemented the theoretical methodology[1] to study surface crossings (decay points) with the same level of accuracy that can be used to study ground-state (or excited-state) transition states. In the case of triplet-sensitized reactions, the final decay point must involve a singlet/triplet crossing, and thus one seraches for the lowest energy point along the N-1 triplet/singlet (T/S) intersection space.[2] Alternatively, when a reaction involves fast radiationless decay from a singlet excited state to singlet ground state (S_1/S_0), one can search for the lowest energy conical intersection point along an N-2 intersection space.[3]

Scheme 1

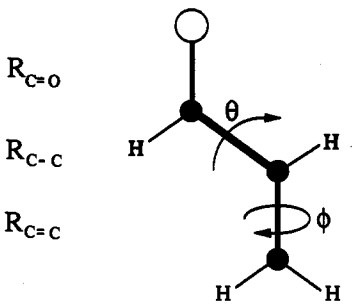

The efficacy of the approach just described has been recently documented in a theoretical study of the description of the main decay points from the first singlet (2^1A_g) excited state to the ground state for both *s-cis*- and *s-trans*-butadiene.[4] There we have been able to find a correlation between the molecular structure (of the *s-cis* and *s-trans* S_0/S_1 conical intersections) at the decay point and the nature and stereochemistry of photoproducts generated. In this paper, the same methodology is applied to the characterization of the surface crossings in acrolein (Scheme 1) in order to provide a model for the photochemistry and photophysics of the carbon–oxygen skeleton of α,β-enones.

The photochemistry of α,β-enones[5] is extremely varied. In addition to the photochemistry of the C=O chromophore (α-

† King's College, London.
‡ "G. Ciamician" dell'Universita di Bologna.
• Abstract published in *Advance ACS Abstracts*, January 15, 1994.

(1) Ragazos, I. N.; Robb, M. A.; Bernardi, F.; Olivucci, M. *Chem. Phys. Lett.* **1992**, *197*, 217.
(2) Yarkony, D. R. *J. Phys. Chem.* **1993**, *97*, 4407.
(3) Atchity, G. J.; Xantheas, S. S.; Ruedenberg, K. *J. Chem. Phys.* **1991**, *95*, 1862.
(4) Olivucci, M.; Ragazos, I. N.; Bernardi, F.; Robb, M. A. *J. Am. Chem. Soc.* **1993**, *115*, 3710.
(5) (a) Schuster, D. I. In *Rearrangements in ground and excited states*; de Mayo, P., Ed.; Academic Press, London, 1980; Vol. 3, pp 167–279. (b) Schuster, D. I. In *The chemistry of enones*; Patai, S., Rappoport, Z., Eds.; John Wiley and Sons: Chichester, U.K., 1989; Vol. 2, pp 693–756.

0002-7863/94/1516-2103$04.50/0

Scheme 2

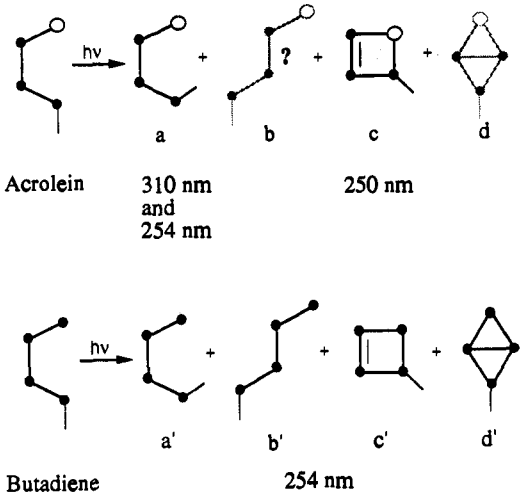

cleavage, H-abstraction, the Paterno–Buchi reaction) and the C=C chromophore (e.g. $[2_\pi + 2_\pi]$ cycloadditions), α,β-enones undergo a variety of photochemical rearrangements of the C=CC=O moiety. Further, in γ-substituted α,β-enones such as cyclohex-2-enones there is also a unique photochemistry of [1,2] sigmatropic shifts (the oxy-di-π-methane rearrangement or the lumiketone rearrangement[5]) of the functional group attached to the γ-carbon. The photophysics (fluorescence/phosphorescence) and photochemistry of α,β-enones are very sensitive to whether the enone is acyclic or cyclic and to whether the solvent is polar or nonpolar.[5] For instance, in the case of cyclic enones, the rigidity imposed on the acrolein moiety by the ring system affects the observed fluorescence and phosphorescence quantum yields and the lifetime of triplet intermediate detected via transient absorption spectroscopy (TAS)[6,7] and time-resolved photoacoustic calorimetry (PAC).[7] In contrast, the photochemistry is often insensitive as to whether direct irradiation or triplet sensitization is used. Clearly, a theoretical model for the C=CC=O moiety in acyclic α,β-enones is a basic requirement for understanding α,β-enone photochemistry in general, and in this paper we focus our attention on the photochemical and photophysical effects associated with the carbon–oxygen skeleton such as *cis–trans* isomerization (a and b in Scheme 2) and ring-closure (c and d in Scheme 2). These same rearrangements also occur in butadiene (a′, b′, c′, and d′ in Scheme 2); however, in this case the triplet states are not involved.

Double-bond *cis–trans* isomerization (product a in Scheme 2) in acyclic α,β-enones has been investigated by Lillya et al.[8] in hexane at room temperature. Irradiation of *cis*- and *trans*-3-penten-2-one at 254 and 313 nm with and without photosensitization (acetophenone and propiophenone) yielded the *trans*- and *cis*-3-penten-2-one, respectively. Despite the fact that slightly smaller quantum yields were obtained with triplet sensitization, this did not lead to dramatic decrease or increase of photoproduct. Further, triplet-quenching does not affect quantum yields of photoisomerization, indicating that in this case a triplet intermediate is short-lived or avoided. A search for a triplet intermediate under the same reaction conditions has been carried out more recently by Schuster, Bonneau, et al.[6,7] Using TAS and other techniques, they have been able to detect (280–310-nm transient absorption) a short-lived triplet intermediate for acyclic (methyl vinyl ketone) and cyclic α,β-enones. The acyclic intermediate had the shortest lifetime (8 ns), and a small but detectable lifetime quenching supports the conjecture that a short-lived triplet intermediate is indeed involved in the photoisomerization reaction.

The ring-closure of acyclic α,β-enones has been studied by Friedrich et al. in the 1970s.[9,10] The authors investigated both the production of oxetenes (c in Scheme 2) and oxabicyclobutanes (d in Scheme 2). They were able to produce an oxetene by direct irradiation of 3,4-dimethyl-3-penten-2-one around 250 nm (450-W medium-pressure mercury lamp through a Vycor filter) in a pentane solution but not using wavelengths above 300 nm (Pyrex filter). Since, at the latter wavelength, one has a large photoisomerization quantum yield, it would appear that the production of oxetene requires either large excess energies or excitation to a higher singlet excited state. Despite various attempts, the same authors were not able to find evidence for the formation of oxabicyclobutane[10] (d in Scheme 2). Thus, it would appear that the bicyclic product does not get formed under the conditions of oxetene production. This behavior of α,β-enones is in contrast with that of butadiene, where cyclobutene and bicyclobutane (c′ and d′ in Scheme 2) get formed simultaneously by 254-nm irradiation in solution.[11]

The lowest energy excited states of α,β-enones are usually denoted in terms of the orbital occupancy as $^1(n-\pi^*)$, $^3(n-\pi^*)$, and $^3(\pi-\pi^*)$. The electronic spectrum of acrolein has been studied frequently, but the assignment of the electronic excitations presents many problems due to the broadness and complexity of the bands and the fact that, being a nonrigid enone, the phosphorescence and fluorescence yields are extremely small. However, the fact that fluorescence (quantum yield 0.007 at 77 K[12]) is detectable at all can be taken as evidence for a stable S_1 intermediate in the $^1(n-\pi^*)$ state in contrast to butadiene, where fluorescence has never been detected.

From emission spectra and theoretical considerations, Becker et al.[12] suggested that photoexcitation of acrolein leads to the $^1(n-\pi^*)$ state (absorption maximum at 330.5 nm), from where the fluorescence (375- and 392-nm maxima) of this compound is produced. The fluorescence is obtained with low yield due to fast internal conversion to S_0 or intersystem crossing to the $^3(n-\pi^*)$ or $^3(\pi-\pi^*)$ states that lie very close to S_1. They also suggest that the $^3(\pi-\pi^*)$ state is stabilized by rotation around the C=C double bond. Thus, at a small rotation angle (ϕ in Scheme 1) this state would cross with $^3(n-\pi^*)$, becoming the lowest triplet state (T_1), with a minimum at a geometry near $\phi = 90°$. Modern spectroscopic methods have yielded similar information about α,β-enones. The $^3(\pi-\pi^*)$ and $^3(n-\pi^*)$ states[6,7,13,14] of rigid α,β-enones appear to lie very close in energy, and the ordering of these two states depends on substituent and solvent effects. The initial photoexcitation leads to the $^1(n-\pi^*)$ after intersystem crossing. Near the twisted $^3(\pi-\pi^*)$ minimum the system would cross with the S_0 state, creating an intersystem crossing channel leading to double-bond *cis–trans* isomerization. The model proposed by Becker[12] gives a rationalization of the low phosphorescence yield (0.000 04 at 77 K with maximum emission at 505 nm) and of the uncertainty in its assignment since the emission would occur from some partially rotated structure, where the interaction between both triplets was strong. Further, the model predicts efficient photochemical *cis–trans* isomerization from $^3(\pi-\pi^*)$ upon excitation above 310 nm and the absence of *s-cis*/

(6) Bonneau, R. *J. Am. Chem. Soc.* **1980**, *102*, 3816–3822.
(7) (a) Schuster, D. I.; Dunn, D. A.; Heibel, G. E.; Brown, P. B.; Rao, J. M.; Woning, J.; Bonneau, R. *J. Am. Chem. Soc.* **1991**, *113*, 6245–6255. (b) Schuster, D. I.; Woning, J.; Kaprinidis, N. A.; Pan, Y.; Cai, B.; Barra, M.; Rhodes, C. A. *J. Am. Chem. Soc.* **1992**, *114*, 7029–7034.
(8) Graf, J. F.; Lillya, P. *Mol. Photochem.* **1979**, *9*, 227–242.
(9) Friedrich, L. E.; Schuster, G. B. *J. Am. Chem. Soc.* **1969**, *91*, 7204–7205.
(10) Friedrich, L. E.; Schuster, G. B. *J. Am. Chem. Soc.* **1972**, *94*, 1193–1199.
(11) (a) Srinivasan, R. *Adv. Photochem.* **1966**, *4*, 113. (b) Ninomiya, I.; Naito, T. *Photochemical Synthesis*; Academic Press: New York, 1989. (c) Squillacote, M.; Semple, T. C. *J. Am. Chem. Soc.* **1990**, *112*, 5546. (d) Leigh, W. J. To be published.
(12) Becker, R. S.; Inuzuka, K.; King, J. *J. Chem. Phys.* **1970**, *52*, 5164–5170.
(13) Block, P. M. L.; Jacobs, H. J. C.; Dekkers, H. P. J. M. *J. Am. Chem. Soc.* **1991**, *113*, 794–801.
(14) Yamauchi, S.; Hirota, N. *J. Phys. Chem.* **1988**, *92*, 2129–2133.

s-trans photoisomerization from T_1. For the flexible enones,[6,7,14] the absence of, or extremely low, phosphorescence is attributed to efficient intersystem crossing from the $^3(\pi-\pi^*)$ state that becomes possible as a result of twisting around ϕ.

Theoretical calculations on acrolein give contradictory information. The early SCF computations (without geometry optimization) of Devaquet[15] attempted to give a global qualitative view of the ground and lowest triplet states, $^3(n-\pi^*)$ and $^3(\pi-\pi^*)$. These results suggested that, after the initial photoexcitation to the $^1(n-\pi^*)$ state, there was a crossing with the $^3(\pi-\pi^*)$ state that in turn crossed with the ground state as ϕ changes to 90°. In contrast, Dykstra[16] concluded that the geometry of the triplet excited states was planar, with an avoided crossing between the $^3(n-\pi^*)$ and $^3(\pi-\pi^*)$ states as the C=C rotation takes place. Lucchese and Schaefer[17] also performed CI calculations, using the optimized geometries obtained by Dysktra, but no further exploration of the shape of the surfaces was done. Valenta and Grein[18] also concluded that the excited states were planar. Finally, we mention the fact that some SCF calculations have been carried out for the *s-cis*/*s-trans* isomerism of acrolein.[19]

Photochemical oxetene formation was assumed to originate from the nonvalence $^1(\pi-\pi^*)$ state reached via excitation in the 254-nm region, although a short-lived triplet intermediate could not be ruled out.[9,10] However, more recent spectroscopic studies on *cis*-acrolein[20] indicate a large vibronic coupling of the S_0 and $^1(n-\pi^*)$ states via a skeletal torsion vibration, so the final stage in the photochemical production of oxetene could occur by decay from the S_1 $^1(n-\pi^*)$ state directly to S_0. There is one extensive MINDO/3 CI study[21] of the photochemical reaction of *s-cis*-acrolein. This work included the computation of nonadiabatic coupling terms between the S_0 and $^1(\pi-\pi^*)/^1(n-\pi^*)$ states. Unfortunately, only idealized coordinate driven reaction paths were used. These results suggest a mechanism where the nonvalence $^1(\pi-\pi^*)$ S_2 state decays near the vertical excitation to the $^1(n-\pi^*)$ state, which in turn decays to S_0 in the last phase of the reaction, leading directly to the oxetene product.

In order to understand the origin of the photophysics and photochemistry of acyclic α,β-enones in general, a detailed knowledge of the nature of the delicate interplay of the $^1(n-\pi^*)$, $^3(n-\pi^*)$, and $^3(\pi-\pi^*)$ potential surfaces for the model acrolein system can provide considerable insight.

Computational Details

All calculations have been performed using the implementation of the CASSCF procedure and the standard 6-31G* basis set available in the Gaussian 92 package.[22] The CASSCF active space comprised six electrons distributed in five orbitals originating from the π and π^* orbitals of the C=C fragment and the π,π^* and n orbitals of the C=O fragment. For equilibrium geometries and transition states, the nature of critical points was confirmed by an analytical frequency computation. The points of surface crossing have been obtained by full optimization of the lowest energy points of crossing between the four relevant states (i.e. S_0, S_1, T_1, and T_2) using the methods described in ref 1 and implemented in a development version of the Gaussian package. In order to obtain other well-defined points on the surface crossings, we have also performed constrained optimizations with $\phi = 0°$ and $\phi = 90°$ in some cases. With these *anchor points* as reference, we have computed some grids in the space $R_{C=O}$, $R_{C=C}$, and ϕ in order to obtain more qualitative information about the way in which the surfaces intersect in many variables.

General theoretical discussion of the nature of surface crossings is given in refs 2 and 23, and we have previously described[1] a computational approach that has been successfully used in several applications.[24] Thus, we shall limit our remarks to a brief summary of the main ideas. For polyatomic systems the real crossing of two potential energy surfaces of the same space–spin symmetry occurs at a conical intersection.[3,23] At a conical intersection geometry, one can identify two directions, $\mathbf{x}_1$ (a vector parallel to the nonadiabatic coupling vector, $\langle\Psi_1|\partial\Psi_2/\partial\mathbf{q}\rangle$) and $\mathbf{x}_2$ (a vector parallel to the gradient difference vector, $\partial(E_2-E_1)/\partial\mathbf{q}$ (where $\mathbf{q}$ is a nuclear displacement vector)). If we plot the energy versus these two directions, the ground- and excited-state surfaces appear as a double cone, with the degeneracy at the common apex of the two half-cones. Movement through geometries residing in the N-2 dimensional subspace orthogonal to $\mathbf{x}_1$ and $\mathbf{x}_2$ (which we shall refer to as the *intersection space*[3]) preserves the degeneracy, and this N-2 dimensional surface will possess its own distinct topology of transition states and minima *etc.* within the reduced dimensionality. For a crossing of a singlet and triplet state, i.e. of two states of different spin symmetry (ignoring spin–orbit terms), the crossing surface is N-1 dimensional with respect to $\mathbf{x}_2$ defined above. The lowest energy point in the N-2 (or N-1) dimensional subspace is a well-defined critical point that is obtained by minimizing the energy under the constraint that the two states are degenerate. One can clearly distinguish the case of an avoided crossing (with a very small energy gap) with a true intersection because the gradient of the excited state vanishes in the former case but not in the later (where only the projection of the gradient in the N-2 space is 0). Obviously, the low-energy regions of the intersection surface are the most energetically accessible and correspond to points where intersystem crossing (via an S/T crossing) or fast internal conversion (via a conical intersection) is more likely to occur. Other points on the intersection surface can be obtained by carrying out the optimization under some suitable geometric constraint. Clearly, intersystem crossing or fast internal conversion can occur at any energetically accessible point on the intersection space.

In order to optimize geometries on the intersection space, one needs to use state-averaged MC-SCF. In this procedure, the orbitals are optimized for an average of the two states involved. Such a procedure is similar in spirit to the averaging over degenerate multiplets that is used in an SCF computation for an open shell atom or linear diatomic molecule.

Finally, we should comment very briefly on the accuracy of our results. CASSCF will give a *balanced* representation of the excited states computed in this work that would not be possible with SCF methods. Thus, the surface topology (minima, transition states, and crossings) should be quite reliable. However, the detailed energetics will be sensitive to the inclusion of dynamic correlation. As we shall discuss in more detail later, ground-state bond lengths agree to 0.01 Å with the experimental ones, but the error of the excited states is slightly larger (e.g. 0.03 Å for $R_{C=O}$). The vertical and 0–0 energies can be taken as an indication of overall accuracy. Our computed vertical excitation energy for the $^1(n-\pi^*)$ state coincides with the middle of the experimental $n-\pi^*$ absorption band. Further, our computed 0–0 energies for $^1(n-\pi^*)$ and $^3(n-\pi^*)$ are underestimated by only a few kilocalories/mole.

Results and Discussion

Since the interplay between the three low-lying excited-state surfaces in acrolein is rather complicated, we begin our discussion with a simplified overview of our results before discussing the details. We have collected all the structural and energetic data in Table 1 and in a schematic representation of the potential

(15) Devaquet, A. *J. Am. Chem. Soc.* **1972**, *94*, 5160–5167.
(16) Dykstra, C. E. *J. Am. Chem. Soc.* **1976**, *98*, 7182–7187.
(17) Lucchese, R. R.; Schaefer, H. F., III; Dykstra, C. E. *Chem. Phys. Lett.* **1977**, *51*, 600–602.
(18) Valenta, K.; Grein, F. *Can. J. Chem.* **1982**, *60*, 601–606.
(19) De Mare, G. R. *Can. J. Chem.* **1985**, *63*, 1672.
(20) Innes, K. K. *J. Mol. Spectrosc.* **1983**, *97*, 420.
(21) (a) Kikuchi, O.; Kubota, H.; Suzuki, K. *Bull. Chem. Soc. Jpn.* **1981**, *54*, 1126. (b) Morihashi, K.; Kubota, H.; Kikuchi, O. *Bull. Chem. Soc. Jpn.* **1985**, *58*, 1083.
(22) *Gaussian 92*; Frisch, M. J., Trucks, G. W., Head-Gordon, M., Gill, P. M. W., Wong, M. W., Foresman, J. B., Johnson, B. G., Schlegel, H. B., Robb, M. A., Replogle, E. S., Gomperts, R., Andres, J. L., Raghavachari, K., Binkley, J. S., Gonzalez, C., Martin, R. L., Fox, D. J., Defrees, D. J., Baker, J., Stewart, J. J. P., Pople, J. A., Gaussian, Inc.: Pittsburgh, PA, 1992.
(23) (a) Von Neunann, J.; Wigner, E. *Phys. Z.* **1929**, *30*, 467. (b) Teller, E. *J. Phys. Chem.* **1937**, *41*, 109. (c) Herzberg, G.; Longuet-Higgins, H. C. *Trans. Faraday Soc.* **1963**, *35*, 77. (d) Herzberg, G. *The Electronic Spectra of Polyatomic Molecules*; Van Nostrand: Princeton, NJ, 1966; pp 442. (e) Gerhartz, W.; Poshusta, R. D.; Michl, J. *J. Am. Chem. Soc.* **1977**, *99*, 4263. (f) Michl, J.; Bonacic-Koutecky, V. *Electronic Aspects of Organic Photochemistry*; Wiley: New York, 1990. (g) Salem, L. *Electrons in Chemical Reactions: First Principles*; Wiley: New York, 1982. (h) Bernardi, F.; De, S.; Olivucci, M.; Robb, M. A. *J. Am. Chem. Soc.* **1990**, *112*, 1737. (i) Bernardi, F.; Olivucci, M.; Robb, M. A. *Acc. Chem. Res.* **1990**, *23*, 405.
(24) (a) Bernardi, F.; Olivucci, M.; Ragazos, I. N.; Robb, M. A. *J. Am. Chem. Soc.* **1992**, *114*, 2752–2754. (b) Bernardi, F.; Olivucci, M.; Robb, M. A. *J. Am. Chem. Soc.* **1992**, *114*, 5805–5812. (c) Bernardi, F.; Olivucci, M.; Ragazos, I. N.; Robb, M. A. *J. Am. Chem. Soc.* **1992**, *114*, 8211–8220. (d) Palmer, I.; Bernardi, F.; Olivucci, M.; Robb, M. A. *J. Org. Chem.* **1992**, *57*, 5081–5087. (e) Palmer, I. J.; Ragazos, I. N.; Bernardi, F.; Olivucci, M.; Robb, M. A. *J. Am. Chem. Soc.* **1993**, *115*, 673–682.

Table 1. CASSCF/6-31G* Energies and Geometries of $(n\text{-}\pi^*)^1$, $(n\text{-}\pi^*)^3$, and $(\pi\text{-}\pi^*)^3$ States

state (label in Figure 1)	energy[a] +190.0	ΔE[b]	geometry (Å) $R_{C=O}$	R_{C-C}	$R_{C=C}$
trans-acrolein					
S_0 planar minimum (A)					
S_0	−0.8236	0.0	1.21	1.48	1.34
$T_1\ ^3(n\text{-}\pi^*)\ ^3A''$	−0.6868	85.84			
$T_2\ ^3(\pi\text{-}\pi^*)\ ^3A'$	−0.6806	89.73			
$S_1\ ^1(n\text{-}\pi^*)\ ^1A''$	−0.6789	90.80			
$^3(\pi\text{-}\pi^*)$ rotated minimum $\phi = 90°$ (B)					
$T_1\ ^3(\pi\text{-}\pi^*)$	−0.7277	60.18	1.22	1.44	1.47
$^3(n\text{-}\pi^*)$ planar minimum (C)					
$T_1\ ^3(n\text{-}\pi^*)\ ^3A''$	−0.7131	69.34	1.35	1.39	1.39
$^3(\pi\text{-}\pi^*)$ planar TS $\phi = 0°$ (D)					
$T_2\ ^3(\pi\text{-}\pi^*)\ ^3A'$	−0.7096	71.54	1.25	1.41	1.51
$^3(n\text{-}\pi^*)$ rotated TS $\phi = 90°$ (E)					
$T_2\ ^3(n\text{-}\pi^*)$	−0.6895	84.15	1.35	1.34	1.48
$S_1\ ^1(n\text{-}\pi^*)$ planar minimum (F)					
$S_1\ ^1(n\text{-}\pi^*)\ ^1A''$	−0.7081	72.48	1.35	1.37	1.40
T_1/T_2 conical intersection $T_2\ ^3(\pi\text{-}\pi^*)/T_1\ ^3(n\text{-}\pi^*)$ $\phi = 0°$ minimum (G)					
$T_1\ ^3(n\text{-}\pi^*)$	−0.7052	74.30	1.32	1.37	1.47
$T_2\ ^3(\pi\text{-}\pi)$ $\phi = 90°$ constrained (H)					
$T_1\ ^3(\pi\text{-}\pi^*)$	−0.6871	85.65	1.40	1.31	1.48
$T_2\ ^3(n\text{-}\pi^*)$	−0.6827	88.41			
$S_0/T_1\ ^3(\pi\text{-}\pi^*)$ intersection (I)					
S_0	−0.7274	60.36	1.22	1.44	1.47
$T_1\ ^3(\pi\text{-}\pi^*)$	−0.7272	60.49			
$S_0/S_1\ ^1(n\text{-}\pi^*)$ conical intersection $\phi = 90°$ minimum (J)					
S_0	−0.6835	87.91	1.40	1.30	1.49
$S_1\ ^1(n\text{-}\pi^*)$	−0.6807	89.73			
$T_1\ ^3(\pi\text{-}\pi^*)$	−0.6907	83.39			
$T_2\ ^3(n\text{-}\pi^*)$	−0.6843	87.41			
$S_0/S_1\ ^1(n\text{-}\pi^*)$ conical intersection $\phi = 0°$ constrained					
S_0	−0.6227	126.06	1.56	1.24	1.69
$S_1\ ^1(n\text{-}\pi^*)$	−0.6197	127.95			
S_1/T crossing $S_1\ ^1(n\text{-}\pi^*)/T_2\ ^3(\pi\text{-}\pi^*)$ $\phi = 0°$ minimum (K)					
$S_1\ ^1(n\text{-}\pi^*)$	−0.7021	75.99	1.34	1.36	1.44
$T_2\ ^3(\pi\text{-}\pi^*)$	−0.7021	76.24			
$T_1\ ^3(n\text{-}\pi^*)$	−0.7072	73.04			
cis-acrolein					
S_0 minimum[c]					
	−0.8211	1.57	1.21	1.48	1.34
$S_1\ ^1(n\text{-}\pi^*)$	−0.6796	90.36			
$T_1\ ^3(\pi\text{-}\pi^*)$	−0.6846	87.22			
$T_2\ ^3(n\text{-}\pi^*)$	−0.6751	93.18			
S_1 minimum[d] (L)					
	−0.7092	71.72	1.36	1.37	1.40
$S_0/S_1\ ^1(n\text{-}\pi^*)$ conical intersection (M) $\phi = 90°$ minimum					
$S_1\ ^1(n\text{-}\pi^*)$	−0.6935	81.64	1.33	1.34	1.49
S_0	−0.6923	82.39			

[a] Energies in hartree. [b] Relative energies in kilocalories/mole. [c] Not fully optimized rms force −0.00045, max force −0.0017. [d] Not fully optimized rms force 0.0020, max force 0.0061.

surface shown in Figure 1 (for *trans*-acrolein only) and in Figure 2. The labels S_0, S_1, T_1, and T_2 are used in the table and the figures to denote the energetic ordering of the states at the tabulated geometries. The electronic nature (i.e. $^1(n\text{-}\pi^*)$, $^3(n\text{-}\pi^*)$, or $^3(\pi\text{-}\pi^*)$) of each structure found is also indicated in Table 1. The labels A–K in Figure 1 refer to the optimized structures in Table 1. We now briefly outline global features of the $^1(n\text{-}\pi^*)$, $^3(n\text{-}\pi^*)$, and $^3(\pi\text{-}\pi^*)$ surfaces and indicate the decay pathways that are important in the photochemistry and photophysics. The only $S_1\ ^1(n\text{-}\pi^*)$ minimum found (point F) is planar ($\phi = 0.0$). After photoexcitation (in absence of triplet sensitizer), *s-trans*-acrolein relaxes to F, mainly by increasing its C=O bond length and decreasing its C–C and C=C bond lengths (see Table 1). From this point the system can relax back to the ground state S_0 via three different routes. The first route involves radiative decay, via fluorescence emission, from the $S_1\ ^1(n\text{-}\pi^*)$ minimum. This decay does not involve formation of new species since, after decay, the system will relax back to the starting reactant. The other two relaxation routes are radiationless and photochemically active. The second route involves radiationless decay via an intersystem crossing (point K in Figure 1a) to the triplet manifold, leading mainly to the production of a short-lived $T_1\ ^3(\pi\text{-}\pi^*)$ twisted intermediate (point B in Figure 1). This intermediate then decays, via a second intersystem crossing (point I in Figure 1b), to the ground state, leading to isomerization of the acrolein double-bond. Finally, the third route involves the singlet manifold only. In this case relaxation to S_0 occurs, from both *s-trans*- and *s-cis*-acrolein, in a single step via decay channels corresponding to S_1/S_0 conical intersections (points J and M in Figures 1 and 2, respectively). Production of oxetene is found to occur exclusively via the singlet path starting from the $S_1\ ^1(n\text{-}\pi^*)$ s-*cis*-acrolein.

The second relaxation route is rather complicated. The first intersystem crossing occurs at the lowest energy S_1/T_2 intersection between the $^1(n\text{-}\pi^*)$ state (point F) and the $^3(\pi\text{-}\pi^*)$ state at a planar geometry (point K) located only 4 kcal mol^{-1} above the S_1 minimum. From the $T_2\ ^3(\pi\text{-}\pi^*)$ sheet the system can access a low-lying T_2/T_1 conical intersection point (point G), which is also planar (see Figure 1a) and which provides a fast radiationless decay channel from T_2 to T_1. Motion from point K to the conical intersection G involves further increase in the original C=C bond length. Thus, *trans*-acrolein can evolve from S_1 to T_1 via an in-plane deformation, which essentially involves a bond order inversion with respect to the ground-state structure. At the conical intersection point G, the two triplet electronic states $^3(n\text{-}\pi^*)$ and

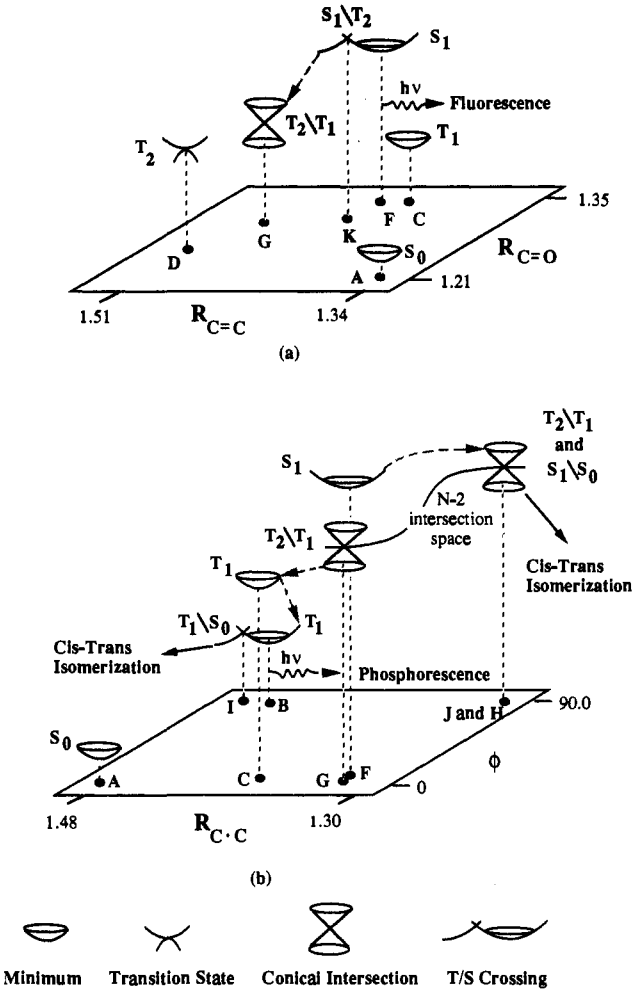

Figure 1. Schematic representation of the optimized structures (stationary and crossing points) on the $^1(n-\pi^*)$, $^3(n-\pi^*)$, and $^3(\pi-\pi^*)$ surfaces of *trans*-acrolein: (a) planar (ϕ = 0.0°) optimized structures along the ($R_{C=C}$, $R_{C=O}$) subspace; (b) two-dimensional cross section along the (R_{C-C}, ϕ) subspace. The bond lengths are in angstroms, and the angles are in degrees. The geometrical parameters are defined in Scheme 1. Dashed arrows indicate excited-state paths, and solid arrows indicate ground-state paths.

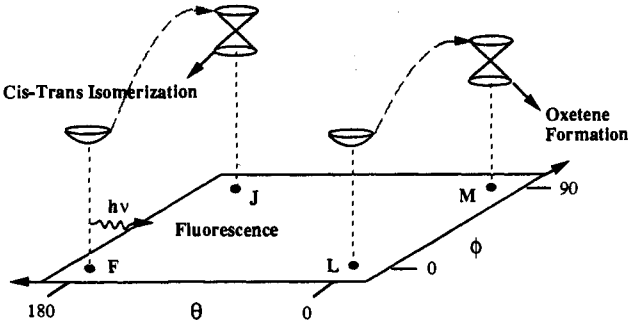

Figure 2. Schematic representation of the optimized structures (stationary and crossing points) on the S_1 $^1(n-\pi^*)$ surface of *s-trans*- and *s-cis*-acrolein. Dashed arrows indicate excited-state paths, and solid arrows indicate ground-state paths.

$^3(\pi-\pi^*)$ are degenerate. Thus, when the system decays at **G** to the T_1 state, it can, in principle, reach two different valleys, as illustrated in Figure 1b. The first valley (on the $^3(n-\pi^*)$ sheet) is centered on the planar $^3(n-\pi^*)$ minimum **C**. The minimum **C** is a planar carbon–oxygen pure diradical structure with a single C–O bond. The second valley belongs to the $^3(\pi-\pi^*)$ sheet and is centered on point **B**. This point corresponds to a highly nonplanar species with a twisted (ϕ = 90°) C=C bond. To reach this structure, the system must simultaneously twist around the original C–C single bond and change the C=O and C–C bond lengths back to the original ground-state values. As we subsequently discuss in some detail, the conical intersection **G** appears to persist even for geometries with a twisted C=C bond. Thus, there is no conventional transition state between **C** and **B**, and **C** decays to **B** via a crossing/recrossing mechanism, which we will discuss in detail subsequently. Further evolution of **B** to the ground state S_0 proceeds via efficient intersystem crossing occurring at the lowest energy T_1/S_0 intersection **I**, located at almost the same geometry as the minimum **B** (see Figure 1b). In acyclic β-substituted α,β-enones this T_1/S_0 decay channel is chemically active as the twisted nature of structure **I** leads to double-bond *cis–trans* isomerization of the original reactant.

The third radiationless decay route for *s-trans*-acrolein is much more direct in comparison to the previous one. This route involves passage through a S_1/S_0 conical intersection **J**, located at about 15 kcal mol^{-1} above the S_1 minimum **F**. Deformation of the system along this route is much more dramatic than the initial deformation to the S_1/T_2 crossing point **K**. This deformation involves the simultaneous 90° rotation about the C=C bond and large changes in the C–C, C=O, and C=C bond lengths. The relaxation of the photoexcited system that follows decay through the conical intersection **J** leads directly to double-bond *cis–trans* isomerization. In fact, like intersystem crossing at point **I**, point **J** has a 90° twisted terminal C–C bond, which allows for isomerization of β-substituted α,β-enones. However, the existence of a larger barrier (lower limit 15 kcal mol^{-1}) from the S_1 minimum to the conical intersection point **J** suggests that this third route may not be effective in conditions of low excess vibrational energy (i.e. when the system is irradiated in solution with 310-nm light). A different, but structurally analogous, S_1/S_0 conical intersection has also been located for *s-cis*-acrolein. In this case the photoexcited *s-cis*-acrolein relaxes to an S_1 $^1(n-\pi^*)$ planar minimum (see point **L** in Figure 2) located about 1 kcal mol^{-1} below the *s-trans* minimum **F**. From this point, the system can reach a *s-cis* S_1/S_0 conical intersection **M** located only 7 kcal mol^{-1} above point **L**, as illustrated in Figure 2. This conical intersection, which can be reached via a pathway similar to that described for conical intersection **J**, appears to provide the radiationless decay channel leading to ring-closure of α,β-enones to oxetenes.

We now proceed to discuss these results in more detail, paying attention to the mechanistic implications for α,β-enone photochemistry and photophysics in general. In section i we will describe the conventional equilibrium structures that have been located in the ground, $^1(n-\pi^*)$, $^3(n-\pi^*)$, and $^3(\pi-\pi^*)$ states. In section ii we will concentrate on the illustration of the complex "triplet" route, which involves two quite different S/T crossings (S_1/T_2 and T_1/S_0) where intersystem crossing can take place and one conical intersection, which allows for ultrafast decay from T_2 to T_1. Finally, in section iii we will describe the "singlet" decay route for both $^1(n-\pi^*)$ *s-trans*- and $^1(n-\pi^*)$ *s-cis*-acrolein, which according to our data, should be active under 250-nm irradiation only.

(i) *s-trans*-Acrolein $^1(n-\pi^*)$, $^3(n-\pi^*)$, and $^3(\pi-\pi^*)$ Equilibrium Structures. Location of the Short-Lived Twisted $^3(\pi-\pi^*)$ Intermediate. The equilibrium/transition structure geometries and energetics found for the ground, $^1(n-\pi^*)$, $^3(n-\pi^*)$, and $^3(\pi-\pi^*)$ state of *s-trans*-acrolein correspond to structures **A–F** in Figures 1 and 2 and Table 1. The CASSCF/6-31G* energies and geometries reproduce the known experimental data reasonably well. The ground-state (**A**) bond lengths agree to 0.01 Å with the experimental ones, but the error in the $^1(n-\pi^*)$ bond lengths is slightly larger (0.03 Å for $R_{C=O}$ to 0.06 Å for $R_{C=C}$).[25-27] The

(25) Hamada, Y.; Nishimura, Y.; Tsuboi, M. *Chem. Phys.* **1985**, *100*, 365–375.
(26) Inuzuka, K. *Bull. Chem. Soc. Jpn.* **1961**, *34*, 729.
(27) Brand, J. C. D.; Williamson, D. G. *Discuss. Faraday Soc.* **1963**, *35*, 184–191.

Scheme 3

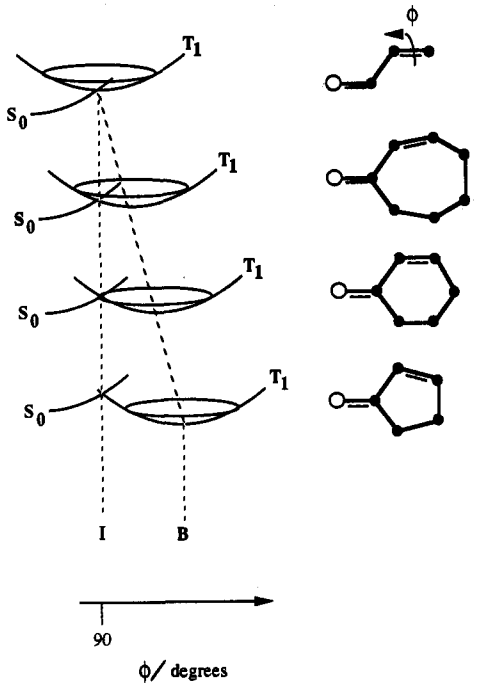

vertical excitation energy to the $^1(n-\pi^*)$ state (i.e. S_0 to S_1) is 90.8 kcal mol^{-1}, which corresponds to an absorption at about 315 nm (i.e. right in the middle of the n–π^* absorption band). Thus, photoexcitation, even with a Pyrex filter, leads to the $^1(n-\pi^*)$ excited state, in agreement with previous assignments. Thus, the observed low quantum yield fluorescence must originate from the only $^1(n-\pi^*)$ minimum found, i.e. point **F**. As far as the 0–0 energies are concerned, we find a gap of 72 kcal mol^{-1} for the S_0 (point **A**) to $^1(n-\pi^*)$ (point **F**) transition and a gap of 69 kcal mol^{-1} for the S_0 to $^3(n-\pi^*)$ (point **C**) transition, in reasonable agreement with the experimental values of 74 and 70 kcal mol^{-1}, respectively.[25-27]

The lowest energy T_1 $^3(\pi-\pi^*)$ minimum (point **B**) is predicted to be twisted ($\phi = 90°$); however, we also find a planar T_2 $^3(\pi-\pi^*)$ transition structure (point **D**) that is very close energetically to the S_1 $^1(n-\pi^*)$ state. This transition structure connects two equivalent minima **B**. In contrast, the lowest T_1 $^3(n-\pi^*)$ minimum (point C) is planar and structurally similar to the S_1 minimum **F**. Further, the $^1(n-\pi^*)$ and $^3(n-\pi^*)$ states have almost the same energy everywhere on the potential surface, with the triplet slightly lower. We also find a $^3(n-\pi^*)$ rotational transition state with $\phi = 90°$ (point **E**) which interconverts two equivalent **C** minima. This transition structure **E** defines a double-bond *cis–trans* isomerization pathway on the T_1 sheet which may be operative in β-substituted α,β-enones by overcoming a 15 kcal mol^{-1} barrier. However, as we will see later, this isomerization route is of little importance due to the possibility of fast interconversion of **C** to the minimum **B** on the T_1 surface.

The existence of a twisted excited state ($^3(\pi-\pi^*)$ point **B**) minimum is of considerable importance for interpreting the very weak phosphoresence and short triplet lifetimes (from TSA and PAC data[6,7]) observed in acyclic and cyclic α,β-enones. However, this implies a hypothesis of a small **C** to **B** energy barrier on T_1 and therefore a rapid rotation from planar to 90° twisted structure in order that one may interpret the observed phosphoresence as originating from the twisted triplet intermediate **B**. We shall return to this point in the next section. However, the experimental data seem to correlate well with this idea. For example the triplet transient lifetime of rigid versus nonrigid α,β-enones, obtained along a series of molecules where the acrolein moiety is embedded in rings of decreasing size, increases when the rigidity of the system is increased. This fact can be explained on the basis of

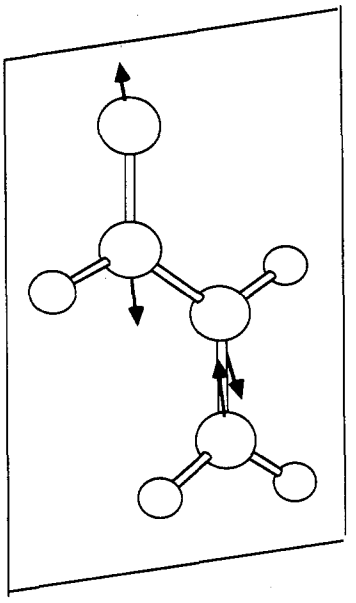

Figure 3. Gradient difference vector $\mathbf{x}_2$ at the minimum energy point of the S_1 $^1(n-\pi^*)/T_2$ $^3(\pi-\pi^*)$ intersection.

Scheme 3. Because of the increase in the rigidity of the system, equilibrium geometry of point **B** must shift toward less twisted structures ($\phi < 90°$). Because of this, the bottom of the **B** well gets displaced from the efficient intersystem crossing region (point **I**) that must occur at a fully twisted geometry ($\phi = 90°$). As a consequence, the lifetime of the (twisted) triplet intermediate corresponding to **B** increases from top to bottom along Scheme 3. Accordingly, the observed short-lived triplet transient absorption at 280–310 nm should be assigned to the twisted $^3(\pi-\pi^*)$ corresponding to **B**, in agreement with the hypothesis of Bonneau[6] and Schuster.[7] However, as we will discuss subsequently, from our computational data, the system can also decay to the $^3(n-\pi^*)$ equilibrium structure **C**, which then interconverts to **B**. Since it is likely that the barrier to this interconversion increases in rigid cyclic α,β-enones, where twisting motion is hindered, we might expect an increase in lifetime for a planar $^3(n-\pi^*)$ intermediate and, in the limit of very rigid systems, it may become the most stable T_1 minimum. This prediction is in agreement with the hypothesis advanced by Schuster,[7b] that 3 $(n-\pi^*)$ may be the lowest energy triplet state in rigid bicyclo-[4.3.0]non-1(6)-en-2-one.

The twisted minimum **B** is thus the most important triplet intermediate along the triplet decay route described above. Once the photoexcited system has reached **B**, it can decay to the ground state, reverting to the planar form and thus, in β-substituted α,β-enones, yielding double-bond isomerization products. We now proceed to discuss the way in which the well **B** gets populated after photoexcitation to S_1.

(Ii) ***s-trans*-Acrolein: the S_1/T_2 $^3(\pi-\pi^*)$, T_2 $^3(\pi-\pi^*)/T_1$ $^3(n-\pi^*)$, and T_1 $^3(\pi-\pi^*)/S_0$ Surface Crossings. Double-Bond *cis–trans* Isomerization.** The triplet radiationless decay path for S_1 starts with a crossing to the triplet manifold. Thus, we begin with a discussion of the S_1 $^1(n-\pi^*)/T_2$ $^3(\pi-\pi^*)$ crossing. The lowest energy crossing point occurs at $\phi = 0°$ (point **K**). The gradient difference vector $\mathbf{x}_2$ is shown in Figure 3, and it is dominated by a C=O stretch and a C=C compression. This S_1 $^1(n-\pi^*)/T_2$ $^3(\pi-\pi^*)$ crossing point is an intermediate structure (a "transition state" when spin–orbit coupling is considered) between the S_1 $^1(n-\pi^*)$ **F** minimum and the T_2 $^3(\pi-\pi^*)/T_1$ $^3(n-\pi^*)$ conical intersection **G**, and the direction of the gradient difference vector is analogous to the direction of negative curvature in a transition state. Along this path $R_{C=O}$ shrinks by 0.03 Å and $R_{C=C}$ increases by 0.07 Å. Note that the energy of the lowest energy $\phi = 0°$ S_1 $^1(n-\pi^*)/T_2$ $^3(\pi-\pi^*)$ crossing **K** is just

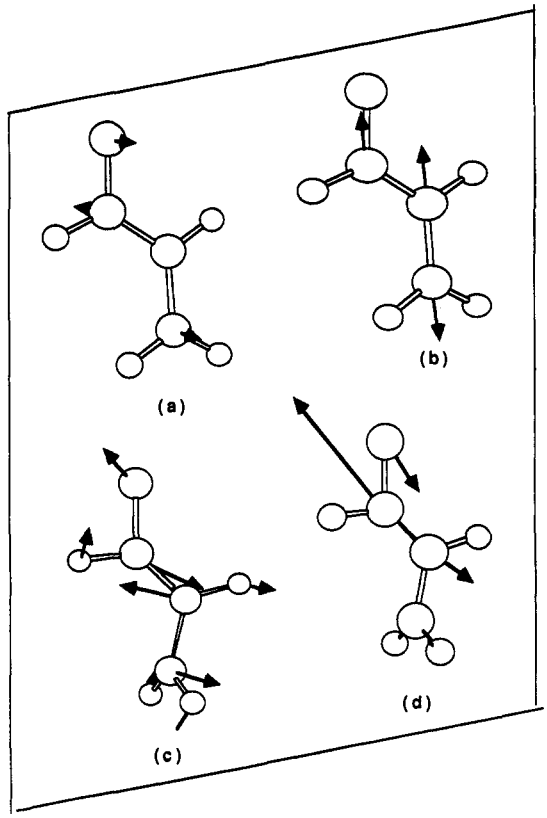

Figure 4. Nonadiabatic coupling $\mathbf{x}_1$ (a, c) and gradient difference $\mathbf{x}_2$ (b, d) vectors for the lowest energy points of the $^3(n-\pi^*)/^3(\pi-\pi^*)$ conical intersection: a, b correspond to point **G** ($\phi = 0°$), and c, d correspond to point **H** ($\phi = 90°$).

4 kcal mol^{-1} above the energy of the S_1 $^1(n-\pi^*)$ minimum **F**, so that decay via the S_1 $^1(n-\pi^*)/S_0$ conical intersection **J** (15 kcal mol^{-1} above the S_1 minimum) cannot compete with the facile intersystem crossing at **K**. Indeed, the S_1 $^1(n-\pi^*)/T_2(\pi-\pi^*)^3$ crossing is usually assumed to occur with unit efficiency.[28]

Since the most efficient decay path from S_1 $^1(n-\pi^*)$ to the triplet manifold occurs at a planar geometry, this process should be efficient in both acyclic and cyclic (rigid) α,β-enones. However, our results show that the next step along the route to S_0, i.e. the decay to T_1, also occurs along a planar deformation coordinate. This decay occurs at a planar ($\phi = 0°$) T_2 $^3(\pi-\pi^*)/T_1$ $^3(n-\pi^*)$ conical intersection point **G**, which corresponds to a fully optimized minimum on the N-2 dimensional T_2/T_1 crossing surface. In Figure 4a,b we give scale drawings that show the structure of **G** and the directions of the vectors $\mathbf{x}_1$ and $\mathbf{x}_2$. On the same N-2 dimensional T_2/T_1 crossing surface (10 kcal mol^{-1} above point **K**) we have also located a twisted ($\phi = 90°$) conical intersection point (point **H**) which has also been fully optimized. This structure is shown in Figure 4c,d together with the corresponding $\mathbf{x}_1$ and $\mathbf{x}_2$ vectors. The points **H** and **G** are two fully optimized points on the N-2 dimensional T_2 $^3(\pi-\pi^*)/T_1$ $^3(n-\pi^*)$ crossing surface. As shown in Figure 1, they partly define the N-2 dimensional intersection line. Obviously **H** cannot be involved in the T_2 to T_1 decay process, which occurs exclusively at the lower energy points on the conical intersection in the region of **G**. However, the fact that **h** exists demonstrates that the T_2 $^3(\pi-\pi^*)/T_1$ $^3(n-\pi^*)$ crossing surface persists as ϕ changes from 0° to 90°. This observation is very important in understanding the relationship between the $^3(n-\pi^*)$ minimum **C** and the twisted $^3(\pi-\pi^*)$ minimum **B**.

When the system deays at T_1/T_2 conical intersection **G**, it can, in principle, reach two different valleys: (1) on the $^3(n-\pi^*)$ sheet, leading to the planar $^3(n-\pi^*)$ minimum **C** and (2) on the $^3(\pi-\pi^*)$ sheet, leading the twisted $^3(\pi-\pi^*)$ minimum **B**. We now give some arguments that show that it is the $^3(\pi-\pi^*)$ minimum **B** that becomes populated and the minimum **C** has only a short lifetime. The argument hinges on the fact that while the initial decay from **G** mainly leads to **C**, there is no true transition state between **C** and **B** because the conical intersection surface persists for $\phi >$ 0°. Since the lowest energy point on the conical intersection lies only 5 kcal mol^{-1} above point **C**, the lowest energy passage from **C** to **B** can only occur via recrossing the conical intersection near point **G**.

The conjecture, that decay from the conical intersection **G** mainly populates the valley leading to minimum **C**, follows from two different observations. Firstly, the motion of the system from point **F** (i.e. the S_1 minimum) to **G** occurs along a planar reaction coordinate. Thus, the system does not accumulate kinetic energy along out-of-plane coordinates, which means that the system will remain on a planar decay pathway. Secondly, the shape of the nonadiabatic coupling and gradient difference vectors $\mathbf{x}_1$ and $\mathbf{x}_2$ shown in Figure 4a,b indicate that there is no component in the termianl CH_2 twisting but the only possible out-of-plane motion involves rotation about the central C–C bond. Furthermore, $\mathbf{x}_2$ essentially coincides with the type of deformation (C=O and C–C stretching accompanied by C=C compression) leading from **G** to **C**.

The question of the existence of a transition state between the $^3(n-\pi^*)$ minimum **C** at $\phi = 0$ and the $^3(\pi-\pi^*)$ minimum **B** at ϕ = 90 is of central importance. We have demonstrated (e.g. the existence of **H**) that the T_2 $^3(\pi-\pi^*)/T_1$ $^3(n-\pi^*)$ crossing surface persists as ϕ changes from 0° to 90°. However, this does not preclude the possibility that the crossing becomes avoided at some point, and a transition state results. TSA data[7] for both acyclic and nonrigid cyclic α,β-enones support the existence of a single T_1 triplet intermediate which is assigned to the $^3(\pi-\pi^*)$ twisted (ϕ = 90 degree) structure. Thus, the observed transient absorption should be due to the T_1 minimum **B** described in section i. However, since only a single transient absorption is assigned to the triplet state T_1, the minimum **C** must be extremely short-lived and undetectable under experimental conditions. This is only possible if the barrier to the transition state from **C** to **B** is very small and close to the bottom of the **C** valley. All attempts to find such a transition state converged to the planar transition state **D** (for rotation around ϕ) on the T_2 $^3(\pi-\pi^*)$ sheet. Thus, one must conclude that there is no way of avoiding the intersection space between the **C** and **B** valleys. The lowest energy point on this intersection space (i.e. the lowest energy conical intersection) will thus provide the reaction bottleneck for the transformation of **C** to **B**.

We can make some progress in understanding the nature of the interplay between the T_2 $^3(\pi-\pi^*)/T_1$ $^3(n-\pi^*)$ intersection space using a simple grid of points. The potential energy surface for T_1 (i.e. the lowest energy triplet state) is shown in Figure 5, where the grid used corresponds to the plane illustrated in Scheme 4. In the center of Figure 5 (i.e. $\phi = 0°$, $R_{C=O} = 1.35$ Å, $R_{C=C} = 1.39$ Å) one has the T_1 $^3(n-\pi^*)$ minimum. At this point the T_2 $^3(\pi-\pi^*)$ state is higher in energy. At the bottom right of the figure (i.e. $\phi = 90°$, $R_{C=O} = 1.22$ Å, $R_{C=C} = 1.47$ Å) one has the T_1 $^3(\pi-\pi^*)$ minimum. The axis labeled "skeletal deformation" has been chosen to include both these points. The ridge between these minima would contain both the transition state (if it existed) and points on the T_2/T_1 N-2 intersection space. The grid plane chosen (see Scheme 4) in Figure 5 excludes the conical intersection point **G**. For a different choice of grid plane, the ridge seen in Figure 5 would curve toward $\phi = 0°$. The $^3(n-\pi^*)$ surface dips just below the $^3(\pi-\pi^*)$ surface at planar geometries $\phi = 0°$, but the $^3(\pi-\pi^*)$ surface is always lower in energy if $\phi \gg 0°$. The interplay between $^3(n-\pi^*)$ and $^3(\pi-\pi^*)$ is further complicated because there is also the $^3(\pi-\pi^*)$ rotational transition state (**D** in Table 1) at $\phi = 0°$, very close to the $^3(n-\pi^*)/^3(\pi-\pi^*)$

(28) Zimmerman, H. E. *Tetrahedron* **1974**, *30*, 1617–1628.

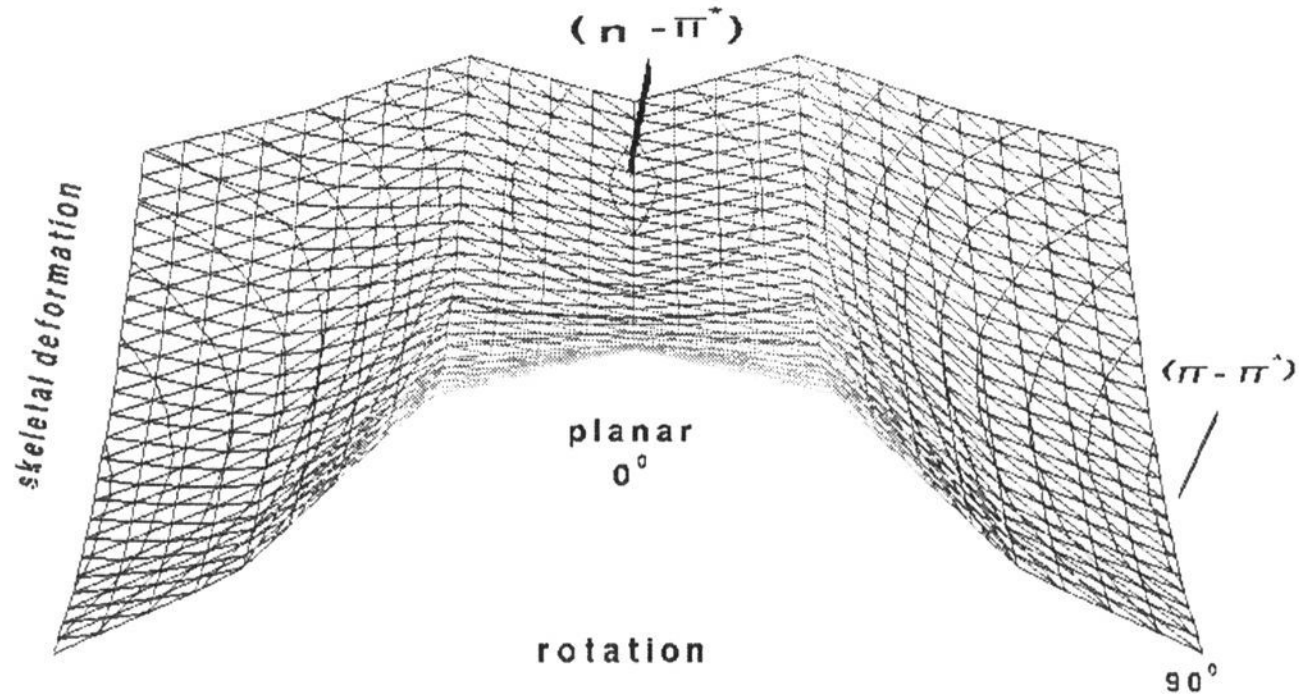

Figure 5. Cross section of the $^3(n-\pi^*)/^3(\pi-\pi^*)$ potential energy surface along ϕ (C=C twisting angle) and $R_{C=O}$, $R_{C=C}$ (skeletal deformation). The grid points are defined via the plane in Scheme 4.

Scheme 4

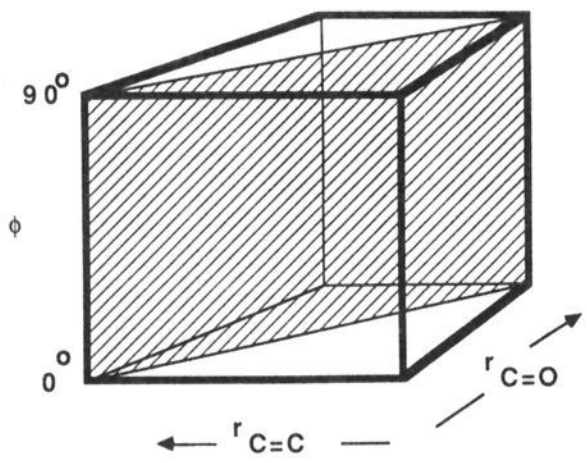

intersection line in the $\phi = 0$ plane. As stated previously, a search for a transition state between **B** and **C** converges, using standard gradient techniques, on this rotational transition state, so one must conclude that the crossing is never avoided in this region.

The nature of the path between the $^3(n-\pi^*)$ **C** and $^3(\pi-\pi^*)$ **B** minima can be seen more clearly in Figure 6. The surface shown in Figure 6 is a surface of constant energy, and the energy is set to the lowest energy point that lies between $^3(n-\pi^*)$ **C** and $^3(\pi-\pi^*)$ **B** minima. The shaded surface is essentially a "rotated" contour line. In such a plot, a transition-state region always shows itself as a "bottleneck". It can be seen that this "bottleneck" is rather "wide" with two "branches", one directed to the $^3(n-\pi^*)$ minima **C** region and the other connecting the two $^3(\pi-\pi^*)$ minima **B**. Thus, the rotational $^3(\pi-\pi^*)$ transition state **D** that connects the two $^3(\pi-\pi^*)$ $\phi = 90°$ minima and the "transition-state region" between the $^3(n-\pi^*)$ and $^3(\pi-\pi^*)$ minima more or less merge very close to **C**. However, there is no true transition state connecting **C** and **B**.

On the basis of this data one is forced to conclude that the lowest energy path between **C** and **B** must traverse the T_2 $^3(\pi-\pi^*)/T_1$ $^3(n-\pi^*)$ crossing surface. The lowest energy point on this crossing (point **G**) is located only 5 kcal mol^{-1} (upper limit) above **C**. The crossing mechanism and its role in the double-bond *cis–trans* isomerization is summarized in Scheme 5. From the conical intersection point **G** the system either decays directly to **B** (if it has some initial vibrational momentum in ϕ) or decays to **C**, then crosses and recrosses the intersection point, and eventually relaxes to **B**. The **C** triplet intermediate is thus extremely short-lived.

Finally, we must discuss the intersection of T_1 $^3(\pi-\pi^*)$ with S_0. The T_1/S_0 intersection **I** occurs near the bottom of the $^3(\pi-\pi^*)$ minimum **B**, in accordance with almost all experimental

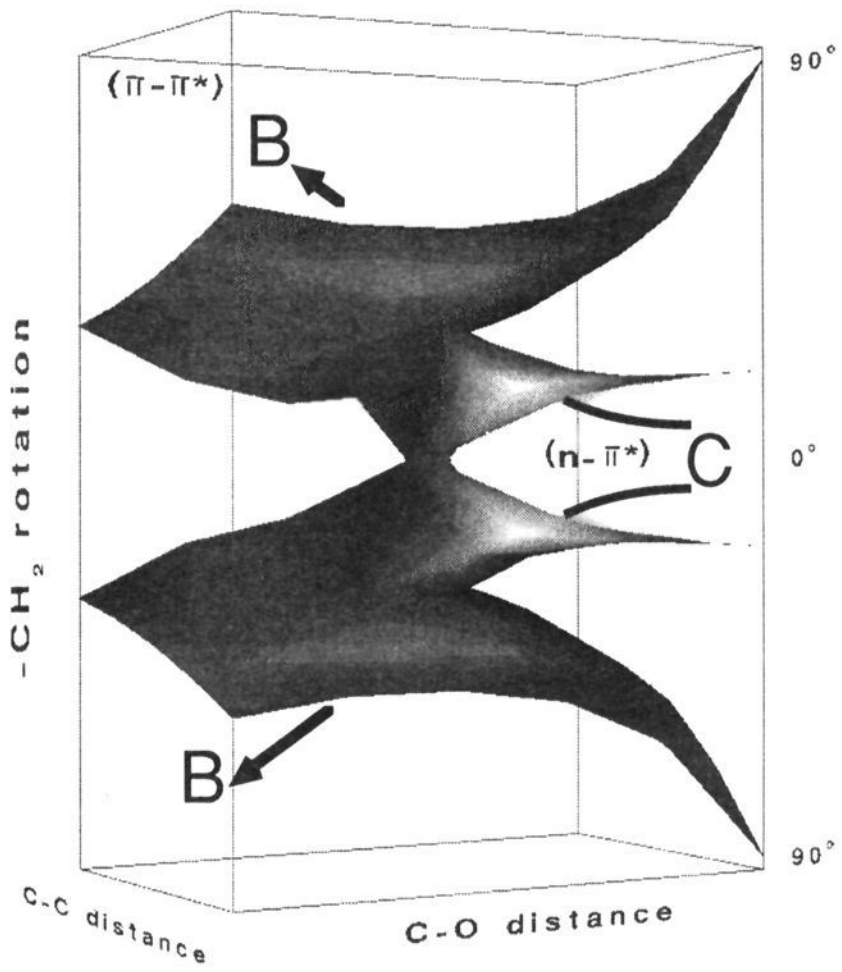

Figure 6. Energy isosurface of the lowest energy triplet states $^3(n-\pi^*)$ and $^3(\pi-\pi^*)$. The *xyz* axes correspond to ϕ, $R_{C=O}$, and $R_{C=C}$. The grid points are defined via the box in Scheme 4. The arrows are intended to indicate the direction corresponding to the direction to the **B** minimum from point **C** through the two "bottlenecks". The "bottleneck" corresponds to the ridge in Figure 5.

data.[5-7,29,30] A scale drawing showing the vector $\mathbf{x_2}$ is given in Figure 7. The minimum of the intersection space is thus virtually coincident with the T_1 $^3(\pi-\pi^*)$ minimum **B**. The vector $\mathbf{x_2}$ corresponds to rotation about ϕ. Since the T_1 $^3(\pi-\pi^*)/S_0$ crossing surface has its minimum near the T_1 $^3(\pi-\pi^*)$ minimum, one might expect that the T/S crossing will be fast in acyclic or nonrigid cyclic α,β-enones (e.g. cycloheptenone; see also the discussion related to Scheme 3). Thus, T/S intersection **I** can be seen as the only effective triplet photochemical reaction channel leading to double-bond *cis–trans* isomerization in β-substituted α,β-enones. In Scheme 5 we illustrate the final part of this reaction

(29) Schuster, D. I.; Brown, R. H.; Resnick, B. M. *J. Am. Chem. Soc.* **1978**, *100*, 4504–4512.

(30) Gilbert, A.; Baggott, J. *Essentials of Molecular Photochemistry*; Blackwell Scientific Publications: Oxford, 1991; p 331.

Scheme 5

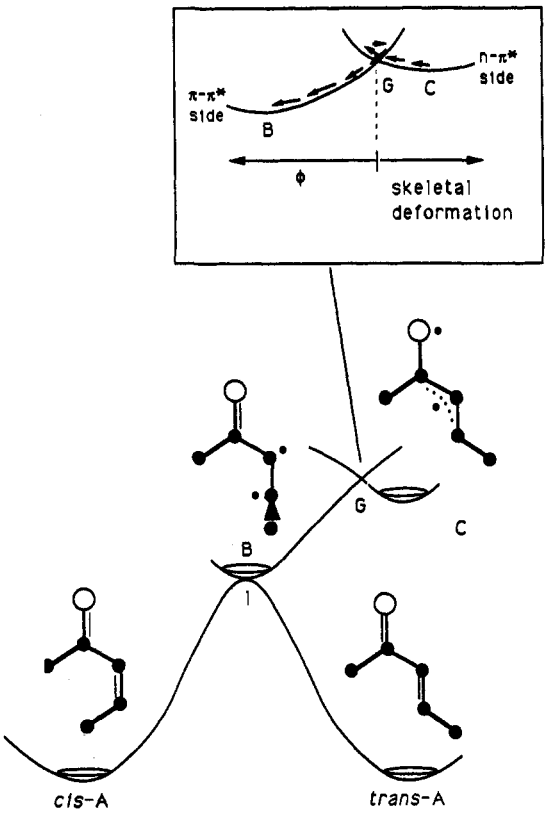

Scheme 6

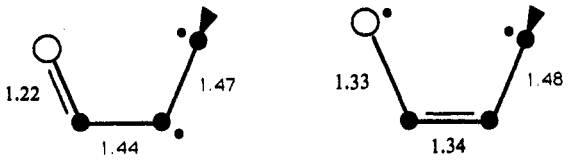

s-cis **B** *s-cis* **J**

pathway (i.e. from T_1 to S_0) in the case of the experimentally tested 3-penten-2-one.[8] In loose cyclic enones such as *cis*-cycloheptenone the formation of a *trans*-ground state cycloheptenone has also been observed as a long-lived absorption at 265 nm which decays via mixed first- and second-order kinetics due to dimerization and ground-state back-formation of the more stable *cis* isomer.[7] The same reaction has been reported for *cis*-cyclooctenone.[31]

The process illustrated in Scheme 5 is consistent with a relatively high quantum yield of double-bond *cis–trans* isomerization. The observed quantum yield ranges from 0.26 to 0.55 in 3-penten-2-one in various solvents (hexane, heptane, pentane) using a 254- or 313-nm light source. This type of quantum yield is due to kinetic energy redistribution, which occurs during the short lifetime of the triplet intermediate (8 ns in vinyl ketone, 11 ns in cycloheptenone).

The computational data presented above also suggest that double-bond *cis–trans* isomers must be the only rearrangement photoproduct of the triplet decay pathway. As we will see in section iii below, this type of reactivity is in marked contrast with that of butadiene, where one has simultaneous production of several photoproducts. Photochemical isomerization about the central C–C bond (i.e. *s-trans* to *s-cis* isomerization) is predicted to be impossible along the triplet pathway due to the rigidly planar geometry at the central C–C bond, which is retained along the pathway of Scheme 5, and the almost complete absence of θ

(31) Eaton, P. E. *J. Am. Chem. Soc.* **1964**, *86*, 2087–2088.

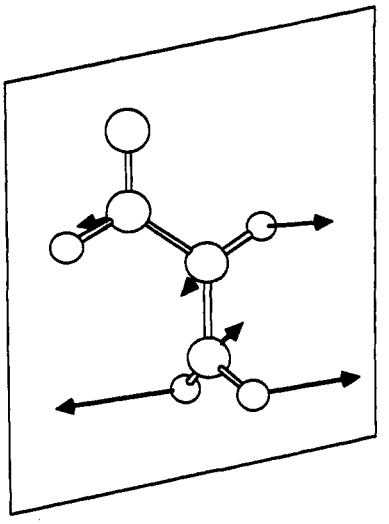

Figure 7. Gradient difference vector x_2 at the minimum energy point of the $^3(\pi\text{–}\pi^*)/S_0$ intersection (point **I**).

components in the vector x_2 of Figure 7. In the case of *s-cis* α,β-enones, the ring-closure to oxetene from the triplet state is also predicted to be impossible due to the geometry and electronic structure of the short-lived triplet intermediate **B**. As shown in Scheme 6 the C=O double-bond is completely formed at the geometry of **B**, which is essentially a triplet diradical with two unpaired electrons centered on the α- and β-carbons. After decay to S_0 the unpaired electrons will recouple to form a new covalent π-bond via rotation of the terminal methylene of acrolein. Oxetene formation on S_0 would require a much more energy-demanding and slow ground-state process involving C=O bond-breaking and bending to form a C–O σ-bond.

There is also an intersection (in the region of point **J** at high energy on the triplet surface) of T_1 $^3(n\text{–}\pi^*)$ with S_0 at $\phi = 90°$ that lies approximately 20 kcal mol^{-1} above the T_1 $^3(n\text{–}\pi^*)$ minimum. We will discuss this point in more detail in the next section, where we demonstrate that at the S_0/S_1 $^1(n\text{–}\pi^*)$ intersection, which occurs for $\phi = 90°$, T_1 $^3(n\text{–}\pi^*)$ is also degenerate with S_0 as a simple consequence of the fact that the $^1(n\text{–}\pi^*)$ and $^3(n\text{–}\pi^*)$ surfaces are degenerate almost everywhere for $\phi = 90°$. The T_1 $^3(n\text{–}\pi^*)/S_0$ intersection for planar geometries occurs at very high energy.

(iii) *s-trans*- and *s-cis*-Acrolein S_1 $^1(n\text{-}\pi^*)$ and S_0 Crossings. Oxabicyclobutane and Oxetene Formation. While double-bond *cis-trans* isomerization in β-substituted α,β-enones occurs at both the 313 or 254 wavelengths, oxetene forms only in low quantum yield from 3,4-dimethyl-3-penten-2-one only when short wavelengths (Vycor filter) are used.[9,10] It has also been reported that the oxetene production is insensitive to the use of butadiene as a triplet quencher[10] and thus that the reaction must involve the singlet manifold only. Accordingly, a different, higher energy, reactive singlet channel must open up when wavelengths around 250 nm are used. On the basis of our computational results this channel should correspond to an S_1 $^1(n\text{–}\pi^*)/S_0$ conical intersection (point **J** in Figures 1 and 2), which has been rigorously located at about 15 kcal mol^{-1} above minimum **F**. In the case of $^1(n\text{–}\pi^*)$ *s-cis*-acrolein (point **L**), we find that an analogous conical intersection exists but in this case it is located at only 10 kcal mol^{-1} above the $^1(n\text{–}\pi^*)$ *s-cis* minimum (point **M** in Figure 2). Thus, irradiation of acyclic α,β-enones at short wavelength would provide the necessary excess energy to reach this alternative singlet decay channel (note that 15 and 10 kcal mol^{-1} represent only lower limits to the S_1 barriers to the conical intersection points since we have not been able to locate transition states in this region because of the near degeneracy). While oxetene can be formed exclusively starting from from *s-cis* α,β-enones, we have seen in Figure 2 that essentially the same type of equilibrium and

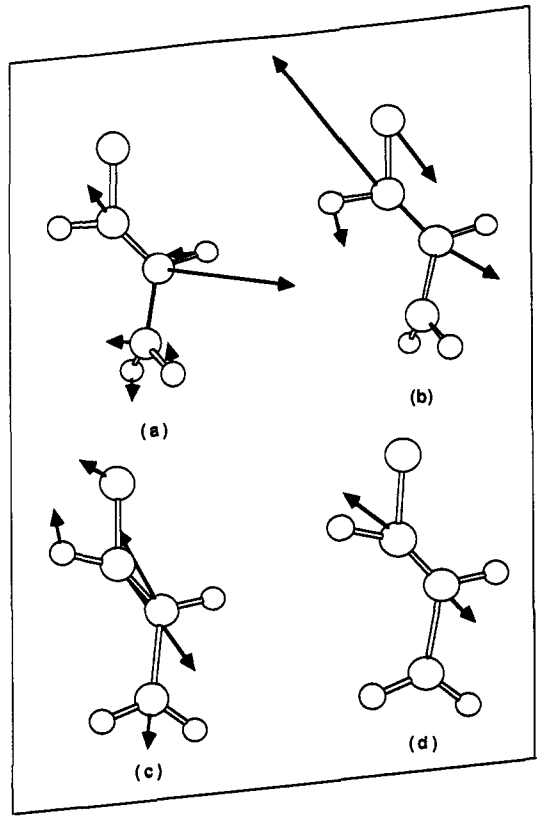

Figure 8. Nonadiabatic coupling $\mathbf{x}_1$ (a, c) and gradient difference $\mathbf{x}_2$ (b, d) vectors for the lowest energy points of the S_1 $^1(n-\pi^*)/S_0$ conical intersection: a, b correspond to point **J** ($\phi = 90°$), and c, d correspond to a (constraint) planar point ($\phi = 0°$).

crossing points exist for both *s-cis*- and *s-trans*-acrolein. Thus, in the following section we will first discuss the salient features of the S_1 $^1(n-\pi^*)/S_0$ crossings in *s-trans*-acrolein.

In *s-trans*-acrolein we have optimized two points on the S_1 $^1(n-\pi^*)/S_0$ intersection space at $\phi = 90°$ (a minimum) **J** and $\phi = 0°$ (constrained). The structural and energetic data are given in Table 1, and the vectors $\mathbf{x}_1$ and $\mathbf{x}_2$ are shown in Figure 8.

From an examination of Figure 8, it is clear that one motion that lifts the degeneracy is rotation about θ and the second corresponds mainly to $R_{C=O}$ compression and R_{C-C} stretch. There are two important points to observe. Firstly, the $\phi = 90°$ crossing minimum **J** lies only 2 kcal mol^{-1} below the S_1 $^1(n-\pi^*)$ vertical excitation energy. Thus, irradiation in the region of 300 nm in solution (vertical excitation energy to $^1(n-\pi^*)$ requires a 315-nm photon) cannot provide enough excess energy to reach the conical intersection. In fact, part of the 17 kcal mol^{-1} vibrational excess energy would be rapidly released to the solvent during the large deformation (from $\phi = 0°$ to $\phi = 90°$) necessary to reach the conical intersection point. Secondly, while the geometry of the S_0/S_1 $^1(n-\pi^*)$ conical intersection has $\phi = 90°$ like the T_1 $^3(\pi-\pi^*)/S_0$ crossing surface minimum, the bond length reversal from the S_0 minimum is extreme ($R_{C=O}$ and $R_{C=C}$ are those of a single-bond, and R_{C-C} corresponds to a fully formed double-bond). The conical intersection point corresponding to $\phi = 0°$ has very high energy indeed and is not accessible. Thus, one can conclude that for nonrigid α,β-enones (i.e. when ϕ is not constrained by the structure) a fast S_1 $^1(n-\pi^*)/S_0$ decay channel is accessible only by overcoming a barrier with a lower limit of 15 kcal mol^{-1}.

The minimum energy point of the conical intersection in the region of the *s-cis* conformation of acrolein occurs at $\theta = 0°$ with $\phi = 90°$ (point **M**). The energetics and geometry of this point are also given in the Table 1, and $\mathbf{x}_1$ and $\mathbf{x}_2$ vectors are shown in Figure 9. The *s-cis* S_1 $^1(n-\pi^*)$ (point **L**) and S_0 energies and geometries are also included in Table 1. The energy of the *s-cis* conical intersection **M** is 7 kcal mol^{-1} lower than that of the

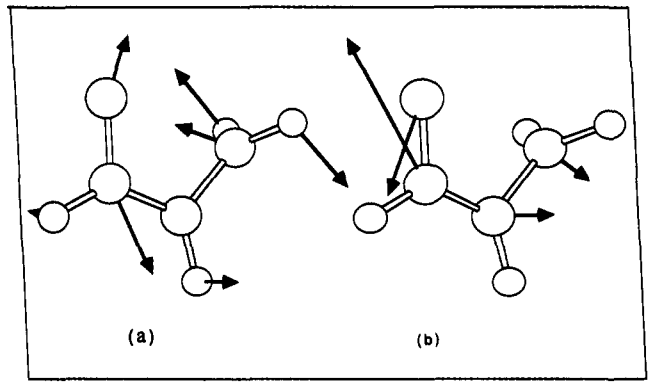

Figure 9. Nonadiabatic coupling $\mathbf{x}_1$ (a) and gradient difference $\mathbf{x}_2$ (b) vectors for the lowest energy point of the S_1 $^1(n-\pi^*)/S_0$ conical intersection for *s-cis*-acrolein (point **M**).

corresponding *s-trans* conical intersection **J**. Excess vibrational energy is required to overcome the 10.10 kcal mol^{-1} (lower limit) barrier to the conical intersection point **M** from the S_1 minimum **L**.

Irradiation at shorter wavelengths should be able to provide the energy necessary to overcome the barriers separating the S_1 $^1(n-\pi^*)$ minima from the respective conical intersection points, thus opening two singlet (one *s-trans* and one *s-cis*) decay channels. Absorption of a 250-nm photon places the system about 160 kcal mol^{-1} above the S_1 $^1(n-\pi^*)$ minima. Here we will not discuss in depth the way in which the barriers to the conical intersections are overcome. However, one might expect that the system would initially be promoted to a nonvalence $^1(\pi-\pi^*)$ state, from where the system can either decay directly to the lowest energy conical intersection point or decay to the $^1(n-\pi^*)$ valley with an initial large vibrational excess energy. The second of these alternatives seems to be the most likely if one considers the TSA results already discussed above. The lifetime of the triplet intermediate, measured for a series of acyclic and cyclic α,β-enones, does not show any change when the system is photoexcited at 353- or 265-nm wavelengths.[7] This implies that the triplet decay channel remains operative (and it is probably the main decay channel) even at short wavelength irradiation. The same trend has been detected in the double-bond *cis–trans* isomerization quantum yield measured using 254- and 313-nm photoexcitation.[8] Thus, we can conclude that, even with 254-nm irradiation, only a fraction of the photoexcited α,β-enone will decay via the singlet S_1/S_0 conical intersection channel and the triplet decay route (described in section ii) will dominate.

The comparison of the computational data related to the *s-trans* and *s-cis* S_1/S_0 conical intersections for acrolein to those already published[4] for butadiene shows that the geometrical and electronic structure of the system at the decay points appears to control the mechanism of the different photoproduct distribution. We conclude by briefly discussing this point. In Figure 10 we show the structures of the conical intersections in butadiene.

In contrast with acrolein, the butadiene conical intersections have a highly nonplanar carbon skeleton. The value of θ is around 130° and 50° for the *s-trans* and *s-cis* structures, respectively. Also, both structures have one C–C–C bending angle with a value near 90°, one completely twisted terminal CH_2 group (i.e. ϕ almost 90°), and one terminal CH_2 group slightly twisted. The electronic structure corresponds to a quasi-tetraradical, where the four electrons of the π-system are only slightly coupled. This electronic structure is a result of the fact that S_1 in butadiene corresponds to a doubly excited $(\pi)^2-(\pi^*)^2$ state, which crosses with S_0. In contrast, the electronic structure of acrolein at the S_1/S_0 conical intersections is diradical, with two unpaired electrons on the O atom and terminal CH_2 carbon.

On the basis of the differences observed in the geometric and electronic structure of *s-cis*- and *s-trans*-acrolein and butadiene

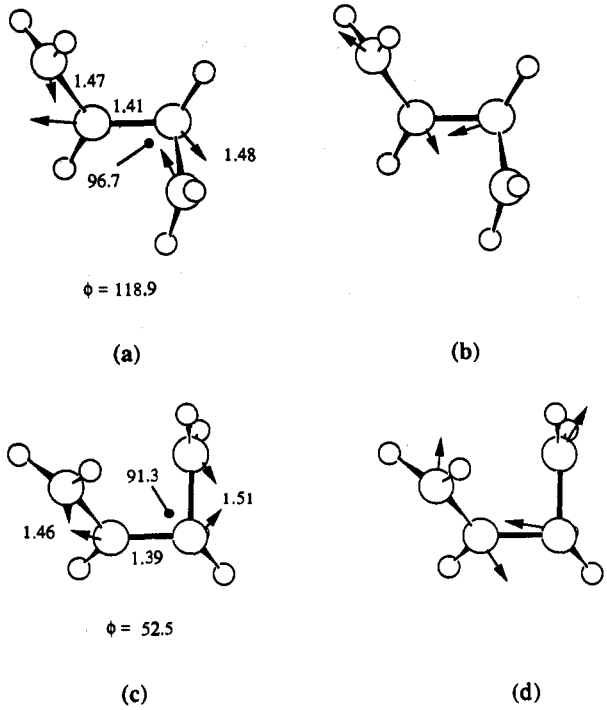

Figure 10. Main geometrical parameters (bond lengths in angstroms and angles in degrees) for the lowest energy points of the S_1 ($(\pi)^2$–$(\pi^*)^2/S_0$ *s-trans* (a, b) and *s-cis* (c, d) conical intersections of butadiene.[4] The arrows in a and c illustrate the direction of the nonadiabatic coupling $\mathbf{x}_1$ vectors, and b and d illustrate the direction of the gradient difference $\mathbf{x}_2$ vectors for these structures.

conical intersections it is possible to rationalize the photoproduct distribution originating from the corresponding decay channels. We first consider the *s-cis* conformer. The diradical nature of *s-cis*-acrolein S_1/S_0 conical intersections leads to the prediction that photochemical *s-cis* to *s-trans* isomerization (product **b** in Scheme 2) could not possibly occur in α,β-enones as a result of irradiation at 254 nm. In contrast to butadiene, the acrolein framework is rigidly planar due to a fully formed double-bond (R_{C-C} = 1.34 Å). Thus, the system starts its relaxation on S_0 at a geometry which will not include a motion about the central C–C bond. Obviously, a possible singlet photoproduct from *s-cis*-acrolein must be that leading to C=O and C=C double-bond back-formation. In this case the 90° twisted terminal CH_2 in the conical intersection structure will rotate back or forward to a planar form, causing double-bond *cis–trans* isomerization (product a in Scheme 2) in β-substituted α,β-enones. This mechanism also operates in butadiene, where one has conical intersections with 90° twisted terminal CH_2 groups. While double-bond *cis–trans* isomerization (product **a'** in Scheme 2) is the fastest process in butadiene photochemistry, *s-trans* to *s-cis* isomerization also occurs rapidly. This behavior is mainly related to the highly twisted (50°) carbon framework of the butadiene conical intersection. The features of the *s-trans*-acrolein decay channel are similar to those described above for the *s-cis* channel. Thus, we expect double-bond *cis–trans* isomerization as the major photochemical process. However, a small fraction of the *s-trans* to *s-cis* product can, in this case, be expected on the basis of the nonadiabatic coupling vector ($\mathbf{x}_1$) of Figure 8, which contains large θ components.

Butadiene irradiation at 254 nm also produces two ring-closure photoproducts: cyclobutene and bicyclobutane (see **a'** and **d'** in Scheme 2). Cyclobutene has been proved to originate exclusively from *s-cis* butadiene,[11c] whereas bicyclobutane is thought to originate from the *s-trans* conformer. While acrolein photoexcitation leads to oxetene (product **c** in Scheme 2), i.e. the four-membered ring analogue of cyclobutene, Friedrich et al. have never been able to detect formation of oxabicyclobutane (product **d** in Scheme 2), i.e. the analogue of bicyclobutane, during short-wavelength (Vycor filter) irradiation of different acyclic α,β-enones.[9,10] This behavior can be explained by comparing the conical intersection structures of *s-cis* and *s-trans* butadiene and acrolein. In fact, the structure of the *s-cis*-acrolein conical intersection favors the ring-closure process to oxetene. The C–O σ-bond formation (involving bending of the O–C–C and C–C–C angles) can occur after the system has decayed to S_0 by spin-recoupling of the O and C unpaired electrons (see Scheme 6). Such a process will occur in competition with double-bond *cis–trans* isomerization. Because the oxetene double-bond along R_{C-C} is already fully formed at the conical intersection geometry, the four-membered-ring formation should be more efficient in acrolein than in butadiene, where a more complex geometrical deformation is required.

The nature of the acrolein conical intersection structures suggests that the formation of bicyclic products from *s-trans* or even *s-cis* geometries will be impossible. The formation of bicyclic products involves the formation of a three-membered-ring diradical that must then close to the bicyclic product. This process is possible in butadiene. In fact, the butadiene conical intersection structures have a C–C–C bending angle with a near 90° value and consequently a certain amount of orbital overlap between positions 1 and 3. In contrast, as a result of the rigidly planar C–O skeleton of the acrolein conical intersection, no 1,3 C–O or 1,3 C–C interaction is possible. Thus, we predict that oxabicyclobutane formation is unlikely in α,β-enones.

Conclusions

The results presented in the previous section support a mechanistic model for the photochemical rearrangement of acyclic α,β-enones based upon two different nonradiative decay routes. The first decay route is already operative at rather long wavelength (around 300 nm) irradiation and involves the formation of a short-lived $T_1\ ^3(\pi-\pi^*)$ 90° twisted triplet intermediate (structure **B** in Figure 1b). This intermediate appears to be formed via a fast $S_1\ ^1(n-\pi^*)/T_2\ ^3(\pi-\pi^*)$ crossing followed by a decay through a $T_2\ ^3(\pi-\pi^*)/T_1\ ^3(n-\pi^*)$ conical intersection **G** or via recrossing from the $T_1\ ^3(n-\pi^*)$ minimum **C**. Photoproducts are then generated starting from structure **B** via decay (intersystem crossing) through a $T_1\ ^3(\pi-\pi^*)/S_0$ crossing point (structure **I**) located at almost the same geometry as the minimum **B**. The second decay pathway avoids the formation of triplet intermediates and occurs exclusively on the singlet manifold via two (*s-cis* and *s-trans*) ultrafast decay channels corresponding to $S_1\ ^1(n-\pi^*)/S_0$ conical intersections. However, these conical intersections are placed 10 and 15 kcal mol^{-1} above the corresponding $S_1\ ^1(n-\pi^*)$ minima for *s-cis*- and *s-trans*-acrolein, respectively. Under these conditions the photoexcited system requires considerable vibrational excess energy to reach the decay points. Thus, the "singlet" decay route opens up only when a shorter wavelength (around 250 nm) is used for the irradiation. Experiments carried out using this wavelength are thus predicted to yield photoproducts which originate from both the "triplet" and "singlet" decay pathways.

The available experimental data seem to agree quite well with the mechanistic scenario presented above. First of all, a short-lived triplet intermediate has been detected as a 280–310-nm transient absorption in acyclic and cyclic α,β-enones irradiated with either 353- or 265-nm light.[6,7] No variation in the measured lifetime of the transient absorption as a function of the irradiation wavelength has been reported. The existence of a twisted triplet intermediate appears to fit well with the photoproduct distribution generated by irradiation of *cis*- and *trans*-3-penten-2-one.[8] Both 313- and 254-nm irradiation of this acyclic α,β-enone lead to the same type of photoproducts with similar quantum yields. Neither the transient absorption data nor the photoproduct distribution data seem to give qualitatively different results when photoex-

citation occurs through triplet sensitizers.[6-8] Finally, the observed variation of transient absorption lifetime with respect to the rigidity of the C–C double-bond involved in the *cis–trans* isomerization reaction can be readily explained on the basis of the magnitude of the energetic barrier to efficient intersystem crossing via the T/S intersection point I (as shown Scheme 3).

From a strictly topological point of view we have concluded that there is no "smooth" reaction pathway between the T_1 $^3(n-\pi^*)$ and T_1 $^3(\pi-\pi^*)$ valleys but that the minimum energy path involves crossing and recrossing of the N-2 dimensional T_2/T_1 intersection space. Thus, the formation of the short-lived T_1 $^3(\pi-\pi^*)$ twisted intermediate (structure **B**) via rearrangement of a possibly ultrashort-lived T_1 $^3(n-\pi^*)$ intermediate (structure **C**) appears to occur via crossing/recrossing of the conical intersection in the region of point **G**, which lies 5 kcal mol^{-1} (upper limit) above **C**. Despite exhaustive attempts, it has not been possible to locate a conventional transition structure describing this transformation. However, in certain rotationally constrained (i.e. rigid) α,β-enones the $^3(n-\pi^*)$ planar **C** minimum could become a more stable energy minimum on T_1.[7b]

While oxetene formation cannot be observed when the irradiation wavelength is above 300 nm, it forms readily when a wavelength around 250 nm is used, as demonstrated in the irradiation of 3,4-dimethyl-3-penten-2-one.[9,10] This behavior is consistent with our findings that oxetene formation occurs exclusively from the *s-cis* α,β-enones via decay from an S_1 $^1(n-\pi^*)/S_0$ conical intersection point located 10 kcal mol^{-1} above the S_1 minimum. Lack of oxabicyclobutane production during irradiation of α,β-enones is also predicted on the basis of the special molecular structure of the S_1/S_0 *s-trans*- and *s-cis*-acrolein conical intersections.

The comparison of the computational data for acrolein to those already published[4] for butadiene shows that the geometrical and electronic structure of the system at the decay points appears to control the mechanism of the related photochemical transformations. In particular, the kind of photoproduct distribution and quantum yields seem to correlate well with the number and special structure of the crossing points (S/T crossings and conical intersections) where the decay actually occurs. This correlation supports the fascinating idea that rigorously determined crossing points play, in photochemistry, a role similar to that of transition states in thermal chemistry.

Acknowledgment. This research has been supported by the SERC (U.K.) under grant numbers GR/G 03335 and GR/G 11941 (CCP1). The authors are also grateful to IBM for support under a Joint Study Agreement. All computations were run on an IBM RS/6000.